# Fatigue damage in fieldshapers used during electromagnetic forming and welding processes at high frequency impulse current

B. Saadouki[1], T. Sapanathan[2, 3, *], PH. Pelca[4], M. Elghorba[1], M. Rachik[2]

[1] Laboratory of Control and Mechanical Characterization of Materials and Structures, National Higher School of Electricity and Mechanics, BP 8118 Oasis, Hassan II University, Casablanca, Morocco

[2] Sorbonne Universités, Université de Technologie de Compiègne, Laboratoire Roberval, CNRS UMR - 7337, Centre de Recherche Royallieu, CS 60319, 60203 Compiègne Cedex, France

[3] Institute of Mechanics, Materials and Civil Engineering, Université catholique de Louvain, B-1348 Louvain-la-Neuve, Belgium

[4] Lebronze alloys – Bornel, 11 rue Ménillet, 60540 Bornel, France

* Corresponding author e-mail : thaneshan.sapanathan@utc.fr

## Abstract

Fieldshapers used in electromagnetic forming and welding processes are prone to have fatigue damage. During each test, impulse current passes through the coil that induces an eddy current cycle and a cyclic Lorentz force on the fieldshaper. Thus, the failure of the fieldshapers during service is associated with the cyclic loading conditions during a decaying high frequency electric current pulse. Repetition of the current pulse that causes the damage and eventually results in a failure which is similar to that occurs during a fatigue problem. Therefore, firstly mechanical and fatigue properties of the new material proposed for the fieldshaper (Siclanic alloy) were characterized. Then various fatigue loading cases with input voltages of 6 – 8.5 kV were investigated to predict the influence of dynamic cyclic loading on the fatigue damage. This study provides a clear understanding of the fatigue damage due to electromagnetic loading and establishes a linear correlation to predict the life cycle for an input electric current. The predicted fatigue damage locations are also in good agreement with the crack formation and their distribution on the filed shapers used in service.

**Keywords :** Fatigue damage, Copper alloy, Fieldshaper, Electric current, electromagnetic impulse

**Nomenclature:**

| | | |
|---|---|---|
| A | : | Elongation at fracture (%) |
| E | : | Young's modulus (*GPa*) |
| K | : | Monotonic hardening coefficient (*MPa*) |
| n | : | Monotonic hardening exponent |
| $N_f$ | : | Number of cycles to failure |
| *UTS* | : | Ultimate tensile strength (*MPa*) |
| R | : | Load ratio |
| Ra | : | Roughness |
| $YS_{0.2\%}$ | : | Conventional yield strength at 0.2% strain (*MPa*) |
| $\sigma_{max}$ | : | Maximum stress (*MPa*) |

## 1. Introduction

High voltage or high current flow in electrical applications require materials to withstand the electrical and electromagnetic forces. In this context, the real challenge is faced when increasing the electrical conductivity of an alloy (e.g. copper alloys or bronze), that adversely affects the mechanical properties. To improve the mechanical properties, precipitation hardening is performed then followed by tempering and quenching steps, which introduces the secondary phase particles in the grains [1-3]. The precipitates impede the movement of dislocations in the sliding plane and thus it improves the mechanical properties [4]. In general, when the precipitates are introduced to improve the mechanical properties, it requires some compromise on its electrical conductivity. For instance, an element such as beryllium used for precipitation hardening in a copper alloy causes a reduction in the electrical conductivity [5].

However, a recent material known by its trade name of "Siclanic" is a promising candidate for the use of electronic, electrical, and electromagnetic applications without compromising the

electrical conductivity for the mechanical properties and vice versa. Siclanic is a Cu-Ni-Si alloy, hardened by the precipitation of $Ni_2Si$ phase [6]. Although various research studies investigated the fatigue behavior of Cu-Ni-Si alloys considering the mechanical loading [7-10], those studies mainly focused on the fatigue behavior based on their microstructural properties. The influences of heat treatments on the fatigue behavior of those alloys were also widely investigated [1, 9, 10]. However, those alloys are made of different amount of chemical compositions than that of Siclanic. Moreover, in the case of an alloy reinforcement by secondary phase precipitations, the particles are sheared by the dislocations which were considered as the main subject of several research studies [11, 12]. That is, in particular for Al-Cu alloys with θ'' precipitates and for Waspaloy alloy (forged nickel) with the presence of fine particles are reported in the literature [11, 12]. However, those studies did not consider the important phenomenon of cyclic softening which occurs after the hardening, and it is reflected by the progressive decrease of the shear modulus between the precipitates and the dislocations.

On the other hand, crack propagation behavior and crack tip softening due to electrical current flow has been investigated by various researchers [13]. Electric current inducing stress around a crack tip had been investigated for a preexisting crack [14, 15]. It was found that the increase in electric current density around the crack tip causing a softening due to Joule effect and this phenomenon could be actively used to control the damage propagation [14, 15]. Numerical simulations also used to investigate the Joule effect on the crack growth behavior under the electro-thermo mechanical loading [16, 17]. The application of high current can affect the behavior of damage in materials directly due to electromigration phenomenon or indirectly by electro-thermo-mechanical phenomena [18]. Electromigration corresponds to a phenomenon of

atoms during the electric current flow; it produces a change in shape of the cavities and which can lead to the rapid destruction of materials. The electro-thermo-mechanical effects come from the temperature increase by Joule effect, and thermally activated phenomena (creep, diffusion, electromigration), then become predominant to lead a failure [19]. Recently, Liu et al. investigated the fatigue crack growth behavior under pulse electric loading [20, 21]. In another study, authors made an attempt to correlate the electric fatigue behavior with generalized Coffin-Manson law [22]. However, damage origin comes from an electrical loading has not been considered.

In contrast, this paper introduces a fatigue damage problem of fieldshaper used for electromagnetic pulse forming and welding (EMPF/EMPW) applications [23, 24]. More detail of the process and load bearing capacity of the fieldshapers are described in Section 2. The fluctuating cyclic loading conditions during the process leads to a fatigue phenomenon. Therefore, various copper alloys are proposed for the fieldshaper and some recent studies also focused on the development of hybrid coils [25]. Nevertheless, until today, the fatigue phenomenon on those fieldshapers is not systematically investigated.

Therefore, a fatigue case study for the Siclanic fieldshaper has been investigated using a strain based fatigue analysis to better understand the scenario of the damage caused in EMPF/EMPW tools. The material properties and Wöhler curve of Siclanic were obtained using both monotonic and fatigue tests, respectively. The fatigue analysis was performed using fe-safe software. To obtain the required stress history during the EMPW process, multiphysics electromagnetic-mechanical simulations were performed prior to the fatigue analysis. The whole study allows

predicting a linear co-relation between the input voltage and fatigue life cycle for the fieldshaper. These results can be used for EMPF/EMPW applications to design the inductor parts to withstand for the fatigue damage resulted from the cyclic input and eddy currents.

## 2. Operational environment and load bearing capacity of fieldshapers

To describe the operational conditions of the fieldshaper and its load bearing capacity, a summary of the EMPF/EMPW is provided in this section. EMPF and EMPW processes spark significant interest in recent years since they offer competitive advantage such as high formability, reduced wrinkling, high productivity and negligible elastic springback compared to other conventional forming methods[24]. Moreover, EMPW offers reliability, flexibility, cost effectiveness and environmental friendliness [26]. These advantages benefit the forming industry and make the process as a real alternative to the conventional forming techniques and other high speed forming methods. It has been reported that the work piece experiences the strain rate of up to $10^2 – 10^4\ s^{-1}$ [27] during the EMPF process while the interface may undergo a significantly high strain rate of up to $10^6 – 10^7\ s^{-1}$ during EMPW [28]. Despite the proven evidence of the contribution of the high strain rate in metal joining, the severe plastic deformation of work pieces has been effectively utilized to produce successful metallic joints in EMPW. As many convincing results exist, the EMPW is suitable for tubular assembly, regular or irregular and flat shape connections. In addition, the process is applicable for a broad range of material combinations such as Cu/Zr metallic glass [29], Al/metallic glass [30], Cu/Manganin [31], flexible circuit boards [32], Cu/Brass, Cu/steel, Cu/Al, Al/steel, Al/Mg, Al/Ni, Al/Fe, Al/Ti and Ti/Ni [33-38] etc.

Fig. 1 shows an illustration of typical magnetic pulse forming unit with an overlap configuration used to weld or crimp a core-clad combination. The unit consists of a pulse generator, a coil and a fieldshaper. The generator contains a transformer, capacitor bank and control switches, which transform a low-voltage power supply into a high voltage. In the case of producing a tubular assembly, the electric discharge from the capacitor bank through an inductive single turn coil generates significantly high Lorentz force on the external tube. It causes the plastic deformation and subsequent collision of the flyer tube onto the fixed inner rod. The discharging pulse frequency is in a range of ∼10-15 *kHz*. The inductive single turn coil and the fieldshaper (Fig. 1) concentrate the magnetic field in the working area. Fig. 1 also indicates the direction of the electromagnetic forces on the tube geometry where the compressive Lorentz force facilitates the deformation of the tube. Moreover, one can control the electromagnetic field and subsequently the deformation of the material using various geometries of the fieldshapers for the same coil geometry [39]. But, in this study a particular geometry of the fieldshaper is considered since it shows significant failure cases in service.

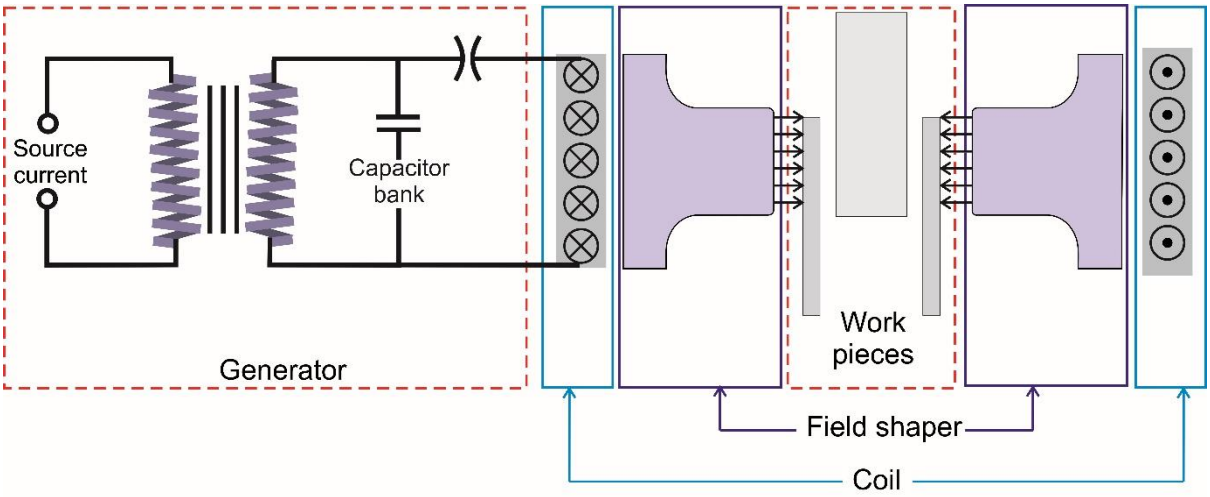


Fig. 1. A schematic illustration showing the EMPF/EMPW unit consisting of a generator, a single turn coil, a fieldshaper, and workpieces (rod and tube). This configuration is typically used for welding or crimping of tubular geometries.

Fig. 2 shows the damaged fieldshapers with cracks and their distributions marked by black arrows. Fig. 2a and b respectively depict a fieldshaper used with multi turn coil made of aluminum alloy and a fieldshaper used with a single turn coil made of a copper alloy. It is also noticeable that the cracks are evenly distributed and mainly concentrated on the opposite side of the slot. The first crack also happens exactly opposite to the slot on the tube side (Fig. 2c).

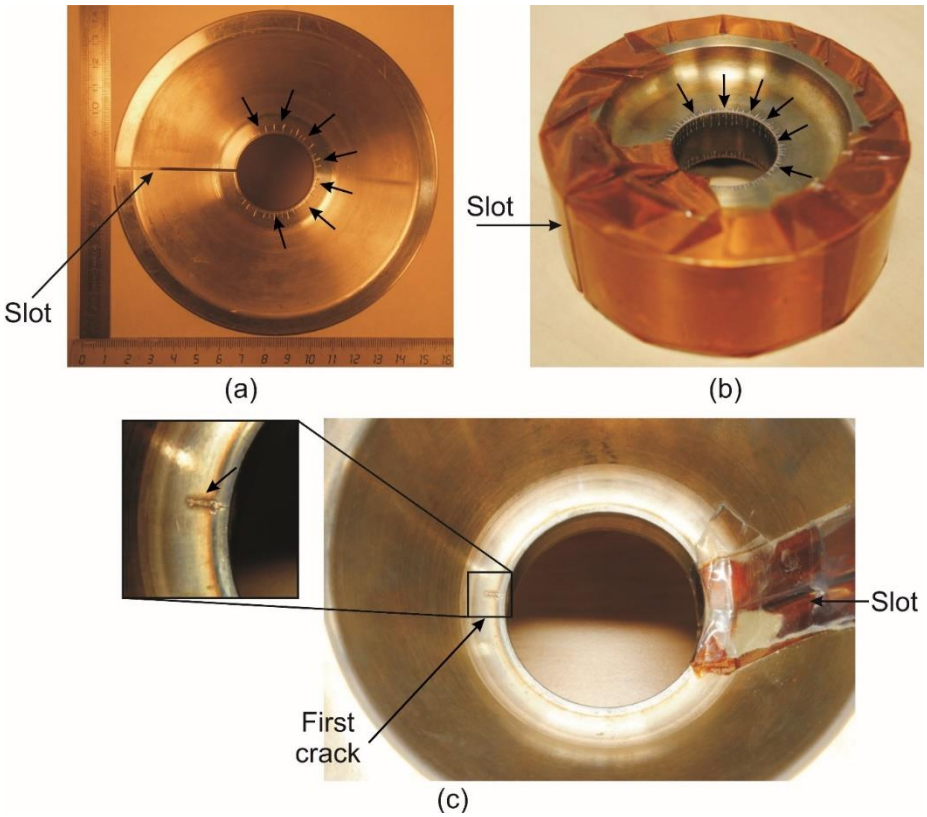


Fig. 2. Cracks (marked by black arrows) and their distribution in the damaged fieldshapers used in service. (a) A fieldshaper used with a multi turn coil made of an aluminum alloy, (b) a fieldshaper used with a single turn coil made of a copper alloy and (c) fieldshaper made of a copper alloy after the first crack that occurs exactly opposite to the slot on the tube side. See Fig. 5 for the complete 3D assembly of a single turn coil with a fieldshaper.

## 3. Experimental work

### *3.1 Materials and method*

The Cu-Ni-Si alloy (Siclanic) used in the present work has the chemical composition of 96.9 % of copper, 2.5 % nickel and 0.6 % silicon in weight percent. The material has been received in bars with 14 *mm* × 14 *mm* × 60 *mm* (W × H × L) in dimension. Each bar allows manufacturing one fatigue sample. Initially longitudinal turning was performed and followed by finishing in a lathe machine. Then numerically controlled machining was used to obtain precise gauge section, chamfering, required threading (for mounting the specimen in the test rig) and final finishing operation to get the sample. Surface polishing was also carried out to meet the standard. To

identify the high cycle fatigue properties, the fatigue tests were carried out according to the ASTM E466-07 standard [40] at CETIM, Morocco on MTS biaxial hydraulic machine.

Schematic representations of the test assembly and the specimen geometry are shown in Fig. 3a and b, respectively. The assembly consists of a rigid frame with an adjustable cross-bar. On the lower part of the frame, two hydraulic cylinders were used to ensure the loading of the specimens. The load cells have the capacity to measure the tensile and compression forces of up to ± 50kN.

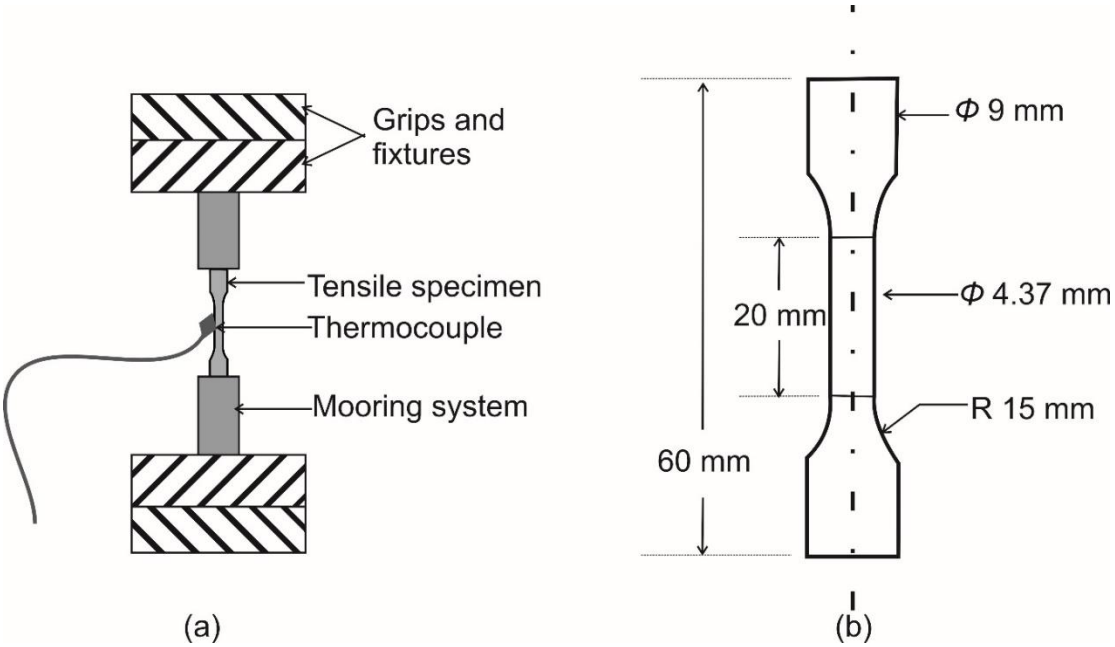


Fig. 3. Schematic illustrations of (a) the experimental apparatus used for the fatigue test and (b) geometry of a Siclanic fatigue specimen.

Fatigue tests were performed with controlled constant stresses (varied between 250 - 500 *MPa* for various tests) with the frequency of 80 *Hz* and load ratio of $R = 0$ at room temperature. In total 13 stress levels were considered. For each stress level, test was repeated 3 times (i.e. 39 tests in total). They instrumented with a thermocouple placed in the middle of the specimen. The

purpose is to control the temperature during the tests and to ensure that the properties were obtained without the influence of thermal effect that could cause thermal solicitation during the failure.

### *3.2. Monotonic tensile and fatigue properties of the material*

Tensile tests were performed to characterize the monotonic properties of the material using a Zwick Roell machine with the displacement mode. An extensometer was used to measure the elongation. Monotonic tensile properties are reported in Table 1.

Table1. Monotonic tensile characteristics of Siclanic

| $E$ $(GPa)$ | $YS_{0.2\%}$ $(MPa)$ | $UTS$ $(MPa)$ | $A$ (%) | $n$ | $K$ $(MPa)$ |
|---|---|---|---|---|---|
| 130 | 498 | 615 | 11.62 | 0.034 | 591 |

Fatigue properties of Siclanic showed a significant dispersion and less repeatability. That is, for the same material under the same load, the lifetime varies during the fatigue characterization. Therefore, a probabilistic Wöhler curve has been established based on the statistical method called the Student Mean Comparison Test [12]. This method allows obtaining the results with 80% confidence interval (i.e. it will give a correct chance of 80 times out of 100 on average for the $N_f$). Fig.4 shows the probabilistic Wöhler curve of Siclanic corresponding to 80% chance of survival.

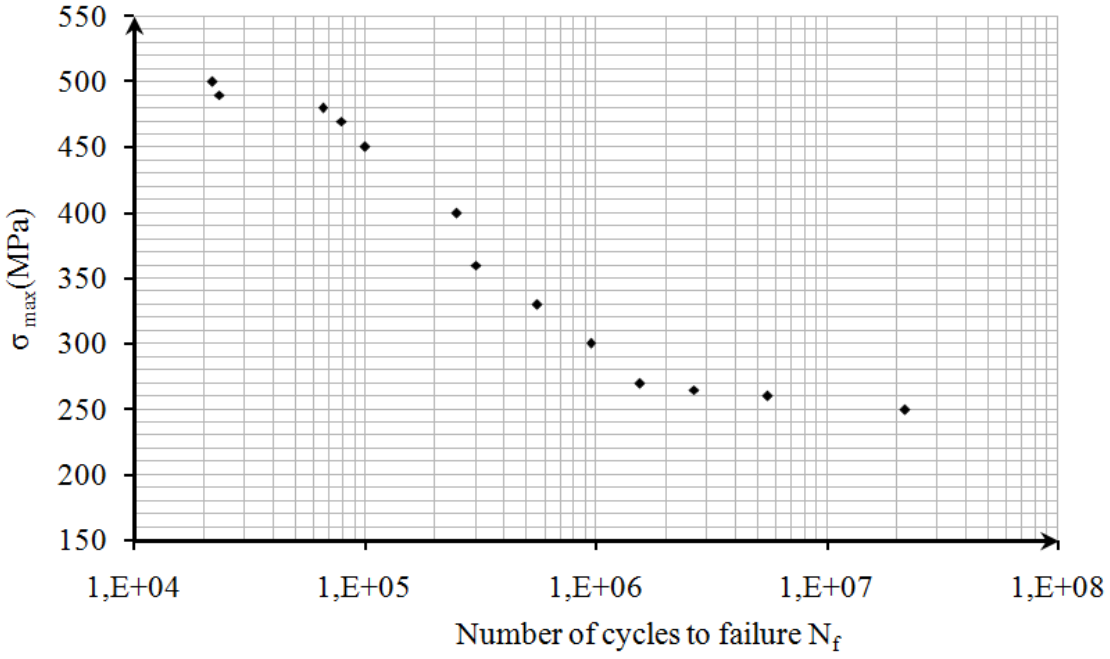


Fig. 4. Probabilistic Wöhler curve with 80% chance of survival for the fieldshaper material, Siclanic.

## 4. Numerical Method

The complete numerical procedure is depicted in Fig. 5 using a flowchart. It involves three main steps: (1) a multiphysics electromagnetic mechanical computation of the welding process to obtain the stress history, (2) The stress history transferred as an ODB file which is readable by the fatigue analysis software and (3) fatigue analysis with the help of fe-safe platform using the previous stress history and experimental fatigue properties of the material. Further details of these steps are given below.

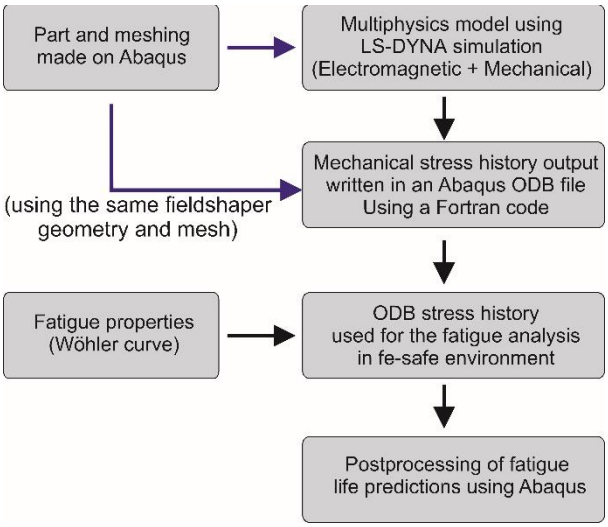


Fig. 5. A flowchart showing the step by step numerical procedures and various tools used in this fatigue analysis.

Firstly, coupled electromagnetic-mechanical simulations are performed using LS-DYNA® package with the solver version R8 to obtain the stress history during the process. The electromagnetic-mechanical solver uses both finite element method (FEM) and boundary element method (BEM) to obtain the solution. The numerical predictions are performed based on Maxwell's equations and Biot–Savart's law to compute the magnetic field and Lorentz forces in LS-DYNA® [41]. BEM is used to evaluate the surface current and electromagnetic field thus the magnetic field in the air is not required in LS-DYNA® simulations. FEM is used during the computation of eddy current and Lorentz force. At each electromagnetic time step, the electromagnetic and mechanical computations are coupled. No additional subroutine was included for the LS-DYNA® calculation.

The one turn coil model with a fieldshaper used in this investigation is shown in Fig. 6a. The detail of the boundary conditions is illustrated in Fig. 6b. The model consists of 8 noded solid elements for both workpieces (rod and tube) and tools (fieldshaper and coil) to handle the electromagnetic calculations in LS-DYNA®. The fieldshaper was modeled with 59 307 brick elements and 63 882

Nodes. The element size was selected based on the skin depth that allows each simulation to accurately capture the electromagnetic skin effect (typically three elements are recommended within the size of skin depth to capture the skin effect and see [42] for more detail of the skin effect). The input currents used in the simulations are given in Fig. 7.

Mechanical and electromagnetic properties used for each component in the simulation are given in Table 2. Although work piece deformation occurs with a high strain rate during the process, preliminary simulations revealed that the stress development on the fieldshaper was not affected by the work piece deformation. Therefore, work pieces were assigned as rigid in this study. Moreover, our earlier investigations (with deformable workpiece) on the thermal effect using an electromagnetic-thermo-mechanical model showed that during an individual test, the local temperature increase in the fieldshaper is about 105 *K*, for the input voltage of 8.5 *kV* [43]. However, since we model the fieldshaper within the elastic region, thermal softening of the material behavior was ignored.

Table 2. Mechanical and electromagnetic properties of various components and their material properties used in the simulations.

| Material | Components | Density ($kgm^{-3}$) | Young's modulus (GPa) | Poison's ratio | Electrical conductivity (IACS%)* |
|---|---|---|---|---|---|
| Aluminium alloy | Tube / Rod | | Rigid | | 30% |
| Siclanic | Fieldshaper | 8900 | 130 | 0.29 | 46% |
| Siclanic | Coil | 8900 | 130 | 0.29 | 46% |
| Polymer | Shock sleeve | 2700 | 13 | 0.29 | Non conductive |

* 100% IACS is equivalent of $5.8001 \times 10^7$ $Sm^{-1}$.

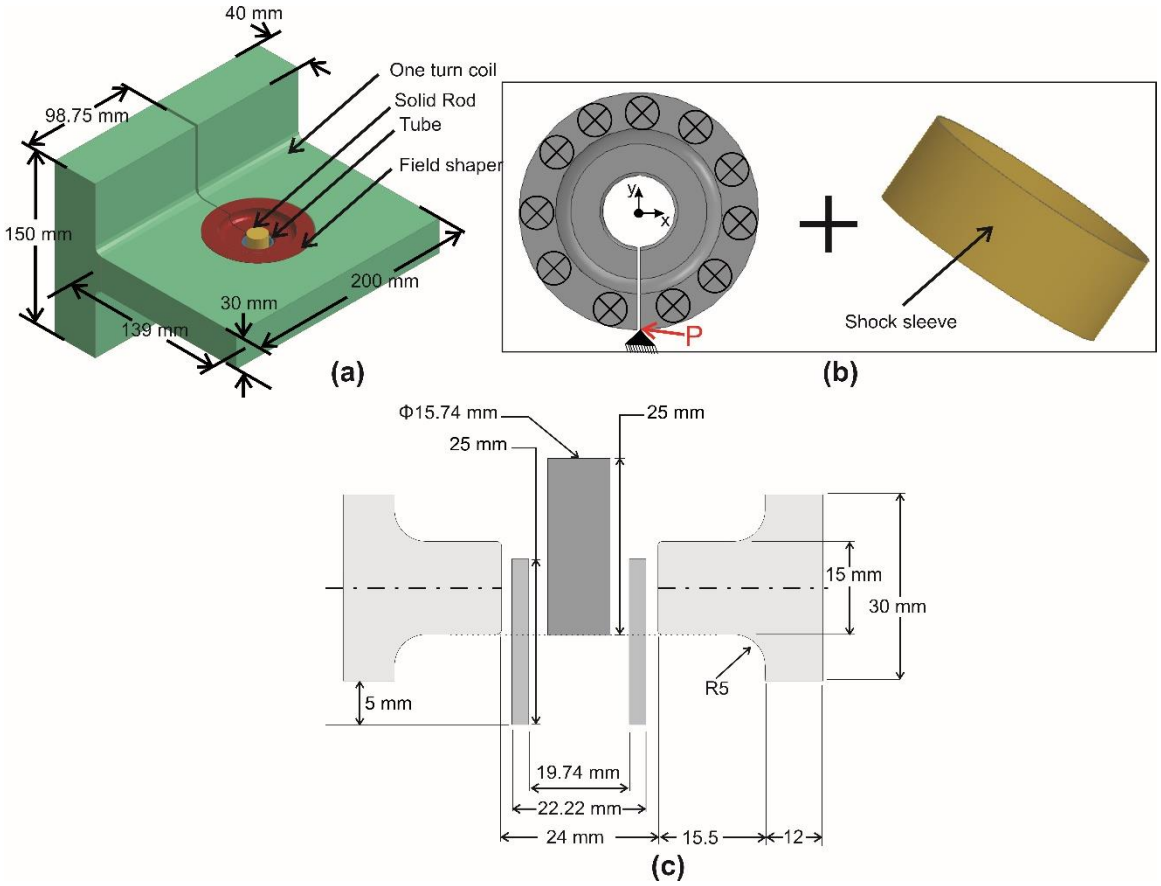


Fig. 6. (a) 3D model used in the coupled electromagnetic-mechanical simulations (b) showing the boundary conditions used for the simulation, where one corner point 'P' was fixed in all directions and the surface indicated by Ⓧ was fixed in z direction (direction normal to the plane). An additional shock sleeve was also added in between the coil and the fieldshaper to represent the reality of the test (i.e. during the test the fieldshaper and coil are separated by a thin polymer film to avoid electrical contact and to maintain the concentricity of the fieldshaper). The shock sleeve was set with 10% yield strength of the field shaper. (c) A schematic illustration showing the cross section of the fieldshaper and workpiece assembly.

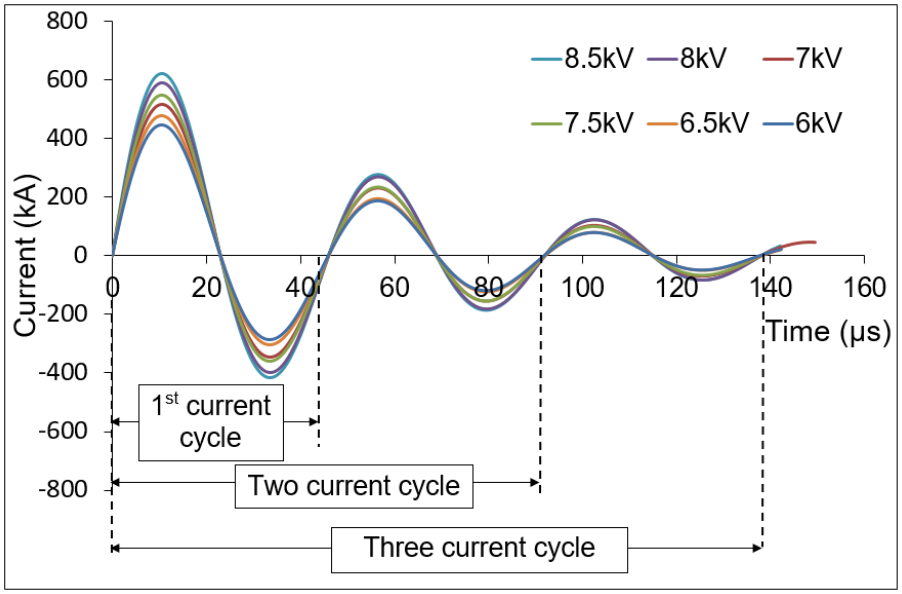


Fig. 7. The input currents with the frequency of ~ 21.5 kHz corresponding to various voltages. These currents were defined with their main three electric current cycles. Various stress histories correspond to the current cycles are used in the fatigue analysis.

The stress history obtained from the multiphysics simulation (result from the FEM of LS-DYNA®) including the mesh was imported to fe-safe environment to predict the fatigue behavior. Other electromagnetic and mechanical field outputs and history outputs were not imported for the fatigue calculation. During this importing step Abaqus environment with a subroutine was used to create the ODB file since the fe-safe do not has the direct import capabilities with the output file of LS-DYNA® until today. Then, the imported stress history was assigned in the fe-safe as the datasets to be read by the software in the analysis environment. The fatigue analysis was performed by setting up the material parameters (including the user defined S-N curve and monotonic parameters of the Siclanic), surface roughness and algorithm. Surface finish was selected from list such as $0.25 \leq Ra \leq 0.6$ µm. The von Mises-Goodman algorithm was used for mean stress correction.

The stress history dataset is defined according to the time corresponding to the electric current cycles (Fig. 7). To compare the effect of current cycles, stress histories corresponding to one, two and three electric current cycles were used in this analysis (Fig. 7).

Once all the settings and parameters are done, fatigue analysis was performed and the worst life repeat and the corresponding failure location details were obtained. The fatigue life cycle was also visualized for the whole model with the log life repeat distribution.

## 5. Results and Discussion

### *5.1 Spatial and temporal distribution of the Lorentz force*

In this section, Lorentz force distributions on the fieldshaper as a function of time and space are presented for the welding case with 8 kV input voltage. Fig. 8 shows the time dependent variation of the Lorentz force at various location of the fieldshaper.

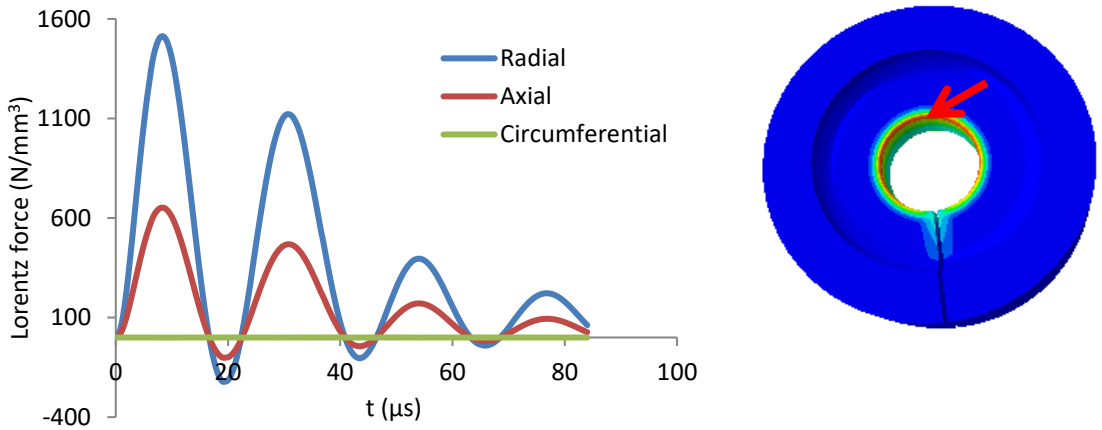


(a)

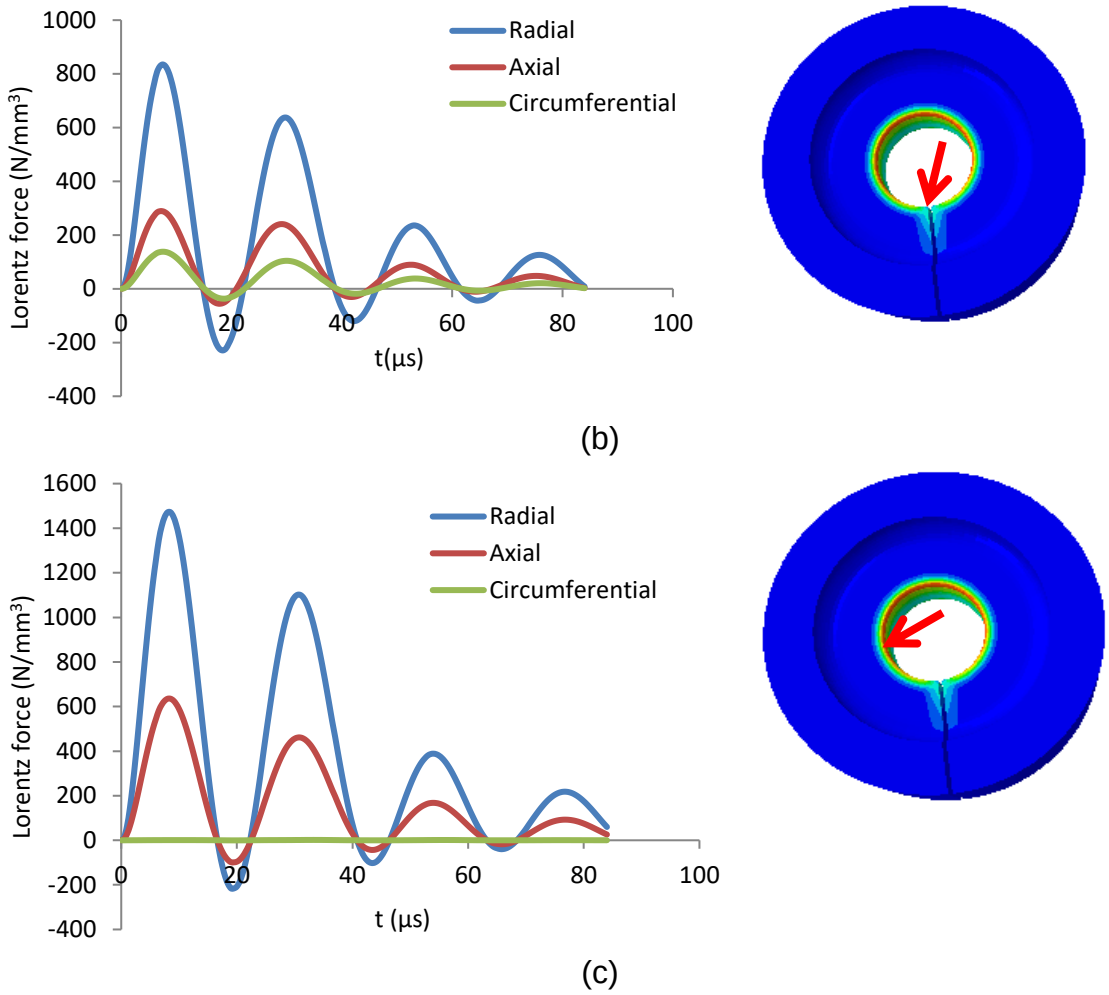


Fig. 8. Time dependent Lorentz force components shown in a cylindrical coordinate system for the Siclanic fieldshaper. The Lorentz force predictions corresponding to three different location at (a) 180° to the slot, (b) 0° to the slot and (c) 90° to the slot. The corresponding locations are pointed out using an arrow on the right side of each plot.

The time dependent non-zero components of Lorentz force also have twice the frequency of the input electric current. This result is also in good agreement with the previous research studies where they confirm the magnetic pressure version has twice the frequency of the input current [44]. That is, from analytical frameworks, one could confirm that the magnetic pressure experienced by the workpiece has twice the frequency of the input current frequency, and it has a direct correlation with the Lorentz force variation in the tools and workpieces [23, 45]. Fig. 8

shows that the radial component of the Lorentz force is dominant and its maximum is located on the opposite side of the slot. It is also as expected based on the theoretical background that the radial component of the Lorentz force should have a larger contribution to deform the workpiece than that of the axial component. The circumferential component of the Lorentz force is negligible except at the slot vicinity. To verify this the force components were plotted with the spatial distribution for the time corresponding to the peak force (Fig. 9). The spatial distribution of the Lorentz force components along the radial and circumferential paths (Fig. 9a) are respectively given in Fig. 9b and c. These variations in the in spatial distribution in agreement with the previous investigation performed by Mamalis *et al.* [46]. In their study, it was also confirmed that the Lorentz forces are high at the opposite to the slot compared to other regions of the fieldshaper [46]. Due to this variation in the Lorentz force because of the presence of the slot, during tube compression, sometime workpiece experience heterogeneous deformations particularly when they undergo large plastic deformations. Moreover, in another resent study, new shape optimized fieldshapers were also proposed to obtain an efficient magnetic pressure distribution inside the working section of the fieldshaper [39].

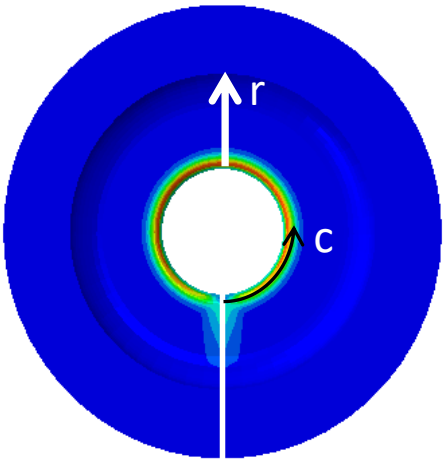


(a)

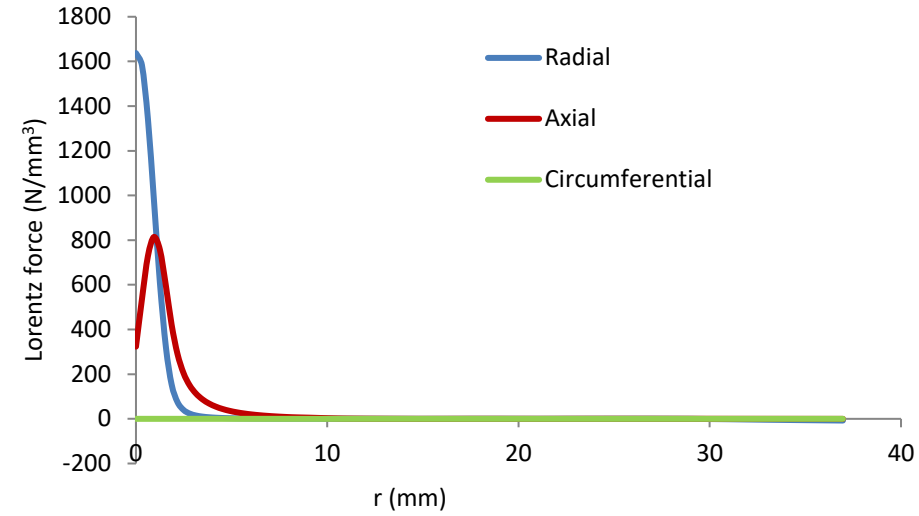


(b)

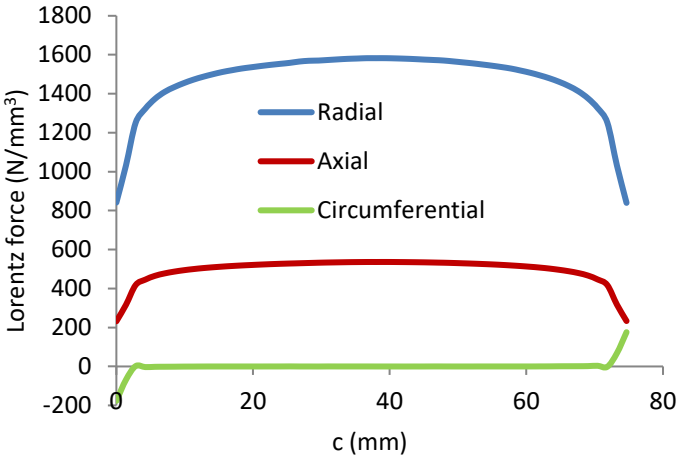


(c)

Fig. 9. Comparison of Lorentz force components in cylindrical coordinate system on space; (a) the fieldshaper marked with two different paths where r and c are indicated for the radial and circumferential directions respectively, (b) Lorentz force components along the radial direction r, and (c) Lorentz force components along the circumferential direction c.

### *5.2. Stress history and fatigue life of the fieldshaper*

The stress development on the fieldshaper was investigated for those six input currents using LS-DYNA® (Fig. 10). Frequency of the stress fluctuation is different in comparison with the input current frequency because of the dynamic effect during the high speed welding process. A comparison of the peak stress history obtained opposite to the slot is given in Fig. 10.

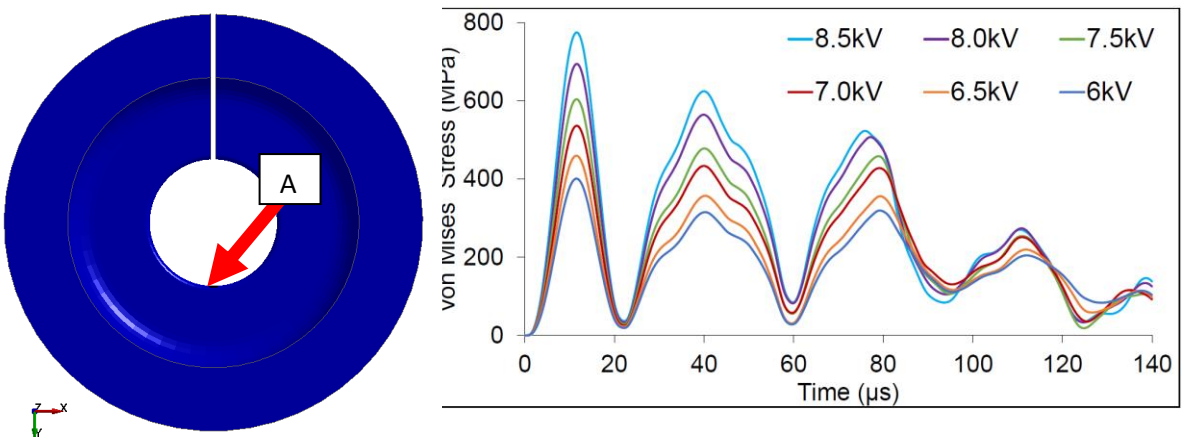


(a) (b)

Fig. 10. (a) Fieldshaper with the Point 'A' marked, and where the stress results are compared for various electric current input and (b) the temporal evolutions of von Mises stresses at the point 'A' for various electric currents.

Due to the large fluctuation of stresses on the tools, the fieldshaper damage is mainly due to fatigue phenomena. Therefore, the stress history was used in the fatigue calculations with fe-safe software. Predictions of the fatigue life cycles corresponding to various stress histories (defined based on electric current cycles as in Fig .7) were analyzed. The fatigue results obtained with 6.0 *kV* and 8.5 *kV* input currents for the Siclanic fieldshaper are respectively shown in Fig. 11 and 12. Appendix A (Supplementary data, Fig. S1 – S4) includes the fatigue prediction results for the currents of 6.5, 7.0, 7.5 and 8.0 *kV*. The model has predicted the shortest life as 6673 (life cycles) with the first current cycle for the case of 6 kV input current (Fig. 11a). It also predicts that the same input current with the stress histories of two and 3 current cycles has the same worst life as 6502 life cycles (Fig. 11b and c). These results indicate that the stress history corresponding to the first current cycle (with the maximum current amplitude) has the most significant effect on the fatigue damage behaviour, while other subsequent current cycles through the coil has a negligible influence on the fatigue life.

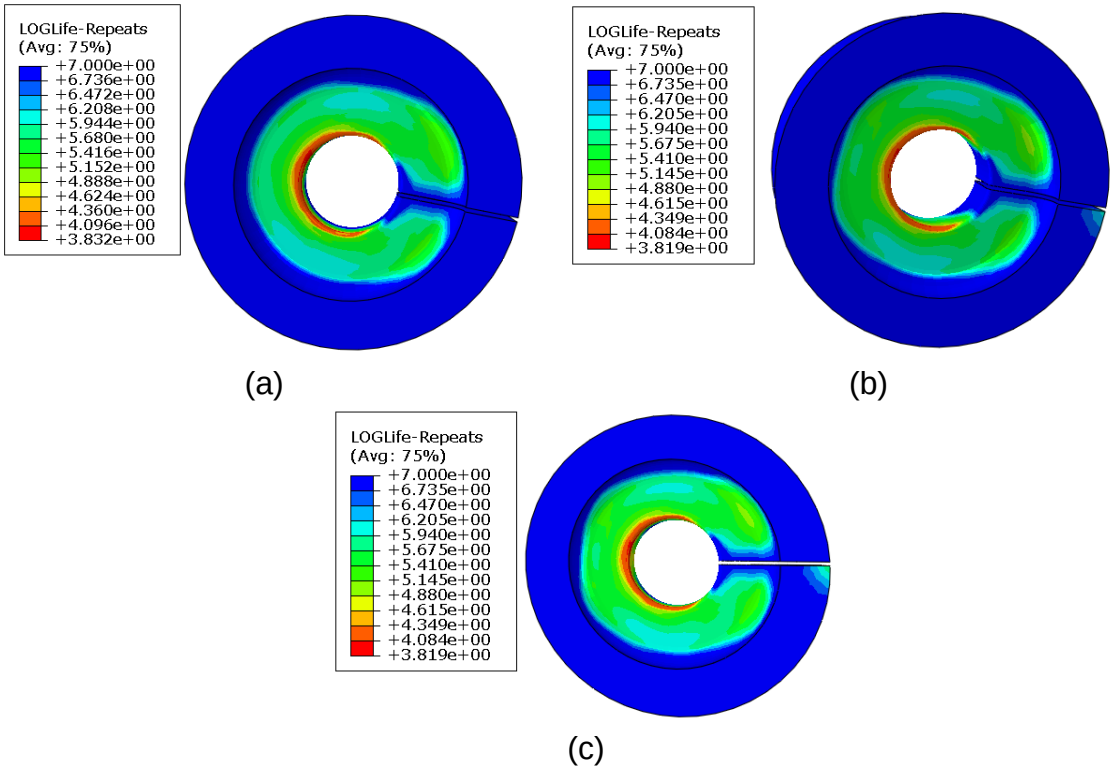


Fig. 11. Predicted fatigue life cycles on the Siclanic fieldshaper for the 6kV input current (a) with the 1st current cycle (b) 2 current cycles (c) 3 current cycles.

The life cycle predictions show the similar trend for all the cases from 6 – 8 *kV*, where the life cycle corresponding to the 1st current cycle is slightly higher than that of the fatigue life cycles corresponding to the two or three current cycles. But, the fatigue life cycle predictions for the case of 8.5 *kV* shows that the worst life repeat corresponding to the 1st current cycle is 436 (Fig. 12a), while the two and three current cycles have the number of worst life repeat of 464 (Fig. 12b and c). However, in all the cases from 6 - 8.5 kV, the fatigue life cycle prediction remains the same for the two and three current cycles compared to the first current cycle.

Experimental observations of the first crack and the worst life repeat prediction from the numerical model coincide as opposite to the slot (Fig. 2c, 11 and 12). However, fatigue crack evaluation was not modelled in this study, and the crack growth could be influenced by the

localized electric current (around the crack tip after the initial crack formation) and the subsequent thermal effect [15, 17]. To model the fatigue failure evaluation, one should consider the thermal effect and material softening, and combination with various temperature dependent fatigue properties obtained for the material to predict the fatigue failure evaluation. From experimental observations cracks continuously form one after other during various experiments (Fig 2a and b). The increase in the number of cracks causes a decrease of the Lorentz force, thus eventually these fieldshapers are not suitable for the process to deliver the required force (to cause sufficient deformation and strain rate).

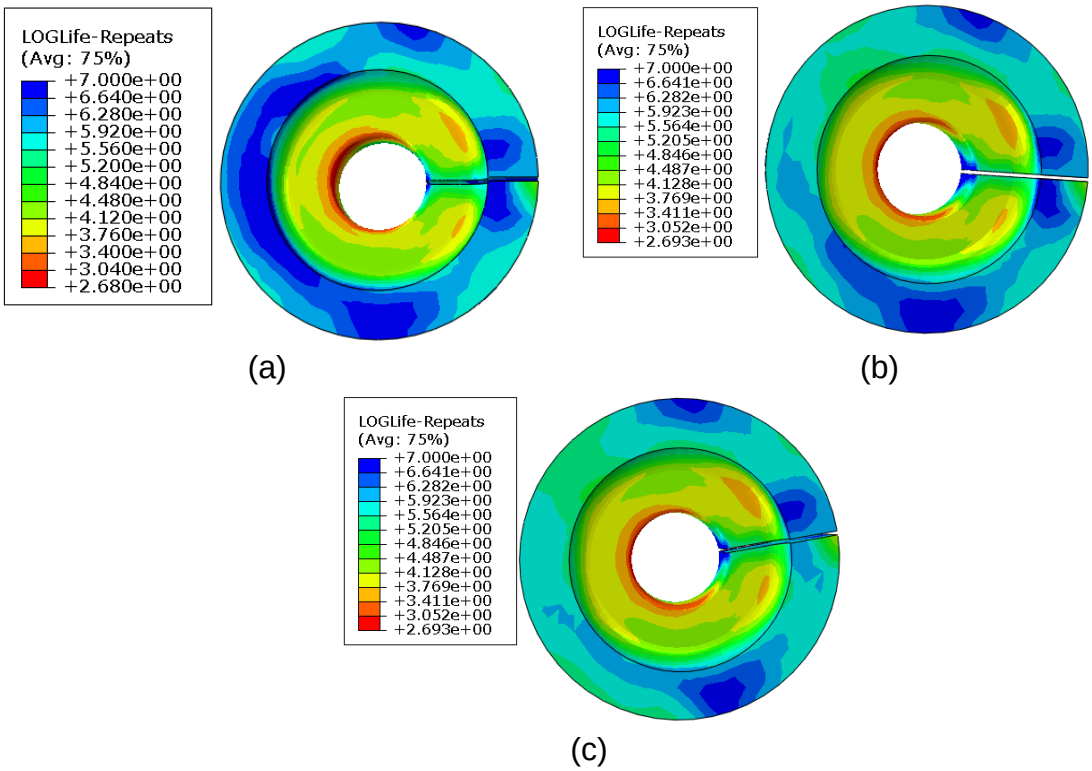


Fig. 12. Predicted fatigue life cycles on the Siclanic field shaper for the 8.5 kV input current (a) with the 1st current cycle (b) 2 current cycles (c) 3 current cycles.

To investigate these variations in the fatigue life cycles prediction, the logarithmic results corresponding to the stress history of 1st current cycle and the two or three current cycles are

plotted against the input voltage as show in Fig. 13. This plot shows a linear evolution with the logarithmic fatigue life cycle and the input voltage. The voltage against the worst life repeat results are also included in the Appendix A (Supplementary material Fig. S5).

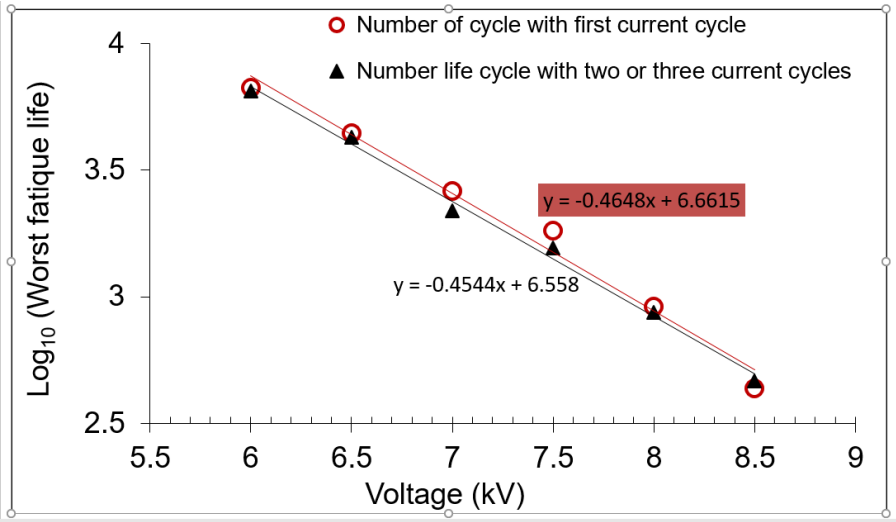


Fig. 13. Siclanic fieldshaper life cycle predictions against the input voltage

It should be noted that these models do not include any residual stresses in the tools due to machining and fabrication processes. However, the residual stresses on the tools can also affect their fatigue life. In this case, inducing a compressive residual stress on the tool is beneficial to improve the fatigue life of the tools. Since the worst life repeat element predicted at the surface level and the crack initiates at the edge of the fieldshaper at the surface and propagate towards the bulk, a surface hardening treatment with a penetration of ~ 100 - 200 µm can be beneficial to improve the fatigue life of the fieldshaper.

Moreover, in an industrial case, initially tools are used with the current pulses of different peak currents to identify the appropriate welding parameters. After that welds are performed for the tested combinations of materials. Therefore, it is not possible to validate the number of fatigue

life cycles with the investigated industrial problem. However, the main purpose of this study is to investigate the fatigue behavior originating from a fluctuating high impulse current and the predictions agree with the failure location. Thus, it could bring more insight to other researchers to seek a fatigue based practical solution during high impulse forming applications.

Besides, continuous multiple tests in an industry can increase the temperature that could cause a thermal softening in the material. In this case, it is very challenging to predict the appropriate stress history for a fatigue calculation and thus one should consider various initial temperatures during each test. In this study, it was assumed that each test is performed independently, and that does not influence the subsequent test. Therefore, the small temperature increase caused during each test does not cause damage initiation.

## 6. Conclusions

Fatigue predictions and tool designs are important when operating under high frequency pulse currents with large amplitudes during electromagnetic forming/welding processes. Being a recent promising candidate, Siclanic is proposed to use in EMPF/EMPW applications without compromising the electrical conductivity for its mechanical properties and vice versa. Although, mechanical characteristics of Siclanic prove that it has sufficiently high monotonic properties, while the process involves cyclic loading that necessitates the fatigue life cycle analysis for the proposed material. Overall finding from this investigation can be summarized as follows;

- Multiphysics simulations showed that the workpieces deformation has a negligible influence on the stresses development of the tools.

- The radial component of the Lorentz force contribute to the large stress development and the effective stress is significantly high at the location opposite to the slot. The circumferential Lorentz force component is negligible in the fieldshaper.
- In terms of fatigue life, the first peak stress, correspond to the first current cycle influence the worst life repeat, while rest of the current cycles show negligible influence on the worst life repeat of the fieldshaper.
- A linear correlation between the logarithmic value of the worst life repeat with the input voltage is established for the Siclanic fieldshaper.
- The predicted damage location using the fatigue analysis concur with the experimental observations of the failed fieldshapers used in service and with the first clack formation that correspond to the element location of the worst life repeat predicted from fe-safe calculation.

## Acknowledgements

Authors acknowledge the funding for COILTIM project from “Région Picardie” and “Le fonds européen de développement économique et régional (FEDER) 2014/2017”. Authors also thank “Plateforme Innovaltech” for its collaboration. TS acknowledges A/Prof. Nicolas Buiron, Université de Technologie de Compiègne, for fruitful discussion on the crack evaluation and thermal effect on the electrical conductors used in EMPF/EMPW processes.

# Appendix A: Supplementary Data

Supplementary data associated with this article can be found, in the online version, at « Please note, that the corresponding DOI link will be specified here later during the production».

# References


[1] S.A. Lockyer, F.W. Noble, Fatigue of precipitate strengthened Cu–Ni–Si alloy, Materials Science and Technology, 15 (1999) 1147-1153.
[2] K.L. Lee, A.F. Whitehouse, P.J. Withers, M.R. Daymond, Neutron diffraction study of the deformation behaviour of deformation processed copper–chromium composites, Materials Science and Engineering: A, 348 (2003) 208-216.
[3] E. Batawi, D.G. Morris, M.A. Morris, Effect of small alloying additions on behaviour of rapidly solidified Cu–Cr alloys, Materials Science and Technology, 6 (1990) 892-899.
[4] E. Hornbogen, Hundred years of precipitation hardening, Journal of Light Metals, 1 (2001) 127-132.
[5] D. Arnaud, J. Barbery, R. Biais, B. Fargette, P. Naudot, Propriétés du cuivre et de ses alliages, Techniques de l'ingénieur. Matériaux métalliques, (2005).
[6] H. Fujiwara, T. Sato, A. Kamio, Effect of alloy composition on precipitation behavior in Cu-Ni-Si alloys, Journal of the Japan Institute of Metals (Japan), 62 (1998) 301-309.
[7] M. Delbove, J.-B. Vogt, J. Bouquerel, T. Soreau, F. Primaux, Low cycle fatigue behaviour of a precipitation hardened Cu-Ni-Si alloy, International Journal of Fatigue, 92 (2016) 313-320.
[8] M. Goto, S. Han, S. Lim, J. Kitamura, T. Fujimura, J.-H. Ahn, T. Yamamoto, S. Kim, J. Lee, Role of microstructure on initiation and propagation of fatigue cracks in precipitate strengthened Cu–Ni–Si alloy, International Journal of Fatigue, 87 (2016) 15-21.
[9] Z. Sun, C. Laitem, A. Vincent, Dynamic embrittlement at intermediate temperature in a Cu–Ni–Si alloy, Materials Science and Engineering: A, 477 (2008) 145-152.
[10] D. Zhao, Q. Dong, P. Liu, B. Kang, J. Huang, Z. Jin, Structure and strength of the age hardened Cu–Ni–Si alloy, Materials Chemistry and Physics, 79 (2003) 81-86.
[11] C. Calabrese, C. Laird, Cyclic stress—strain response of two-phase alloys Part I. Microstructures containing particles penetrable by dislocations, Materials Science and Engineering, 13 (1974) 141-157.
[12] R. Stoltz, A. Pineau, Dislocation-precipitate interaction and cyclic stress-strain behavior of a γ′ strengthened superalloy, Materials Science and Engineering, 34 (1978) 275-284.
[13] Y.I. Golovin, V.M. Finkel, A.A. Sletkov, Effects of current pulses on crack propagation kinetics in silicon iron, Strength of Materials, 9 (1977) 204-210.

[14] G.X. Cai, F.G. Yuan, Stresses around the crack tip due to electric current and self-induced magnetic field, Advances in Engineering Software, 29 (1998) 297-306.
[15] G.X. Cai, F. Yuan, Electric current-induced stresses at the crack tip in conductors, International journal of fracture, 96 (1999) 279-301.
[16] T.J.C. Liu, Thermo-electro-structural coupled analyses of crack arrest by Joule heating, Theoretical and Applied Fracture Mechanics, 49 (2008) 171-184.
[17] S. Satapathy, F. Stefani, A. Saenz, Crack tip behavior under pulsed electromagnetic loading, in: Electromagnetic Launch Technology, 2004. 2004 12th Symposium on, IEEE, (2005) 106-110.
[18] C. Basaran, M. Lin, H. Ye, A thermodynamic model for electrical current induced damage, International Journal of Solids and Structures, 40 (2003) 7315-7327.
[19] M. Risbet, E. Hug, N. Buiron, Interactions entre propriétés thermomécaniques et propriétés électriques d'alliages Ni-20Cr de faibles épaisseurs, in: 17ème Congrès Français de Mécanique, Troyes, France, (2005) 1-6.
[20] H.Q. Lin, Y.G. Zhao, Z.M. Gao, L.G. Han, Effects of pulse current stimulation on the thermal fatigue crack propagation behavior of CHWD steel, Materials Science and Engineering: A, 478 (2008) 93-100.
[21] J. Shieh, J.E. Huber, N.A. Fleck, Fatigue crack growth in ferroelectrics under electrical loading, Journal of the European Ceramic Society, 26 (2006) 95-109.
[22] X. He, J.Y. Fu, Experimental evidence that electrical fatigue failure obeys a generalized Coffin–Manson law, Physics Letters A, 381 (2017) 1598-1602.
[23] V. Psyk, D. Risch, B.L. Kinsey, A.E. Tekkaya, M. Kleiner, Electromagnetic forming—A review, Journal of Materials Processing Technology, 211 (2011) 787-829.
[24] T. Sapanathan, R.N. Raoelison, N. Buiron, M. Rachik, Magnetic Pulse Welding: An Innovative Joining Technology for Similar and Dissimilar Metal Pairs, in: M. Ishak (Ed.) Joining Technologies, InTech, Croatia, (2016) 243-273.
[25] D. Risch, J. Nebel, V. Psyk, E. Vogli, W. Tillmann, A. Tekkaya, Hybrid material design for coils used in electromagentic forming processes, in: Proceedings of the 7th International Conference "*THE*" Coatings in Manufacturing Engineering, Chalkidiki, Greece, (2008) 269-278.
[26] A. Kapil, A. Sharma, Magnetic pulse welding: an efficient and environmentally friendly multi-material joining technique, Journal of Cleaner Production, 100 (2015) 35-58.
[27] J.R. Johnson, G. Taber, A. Vivek, Y. Zhang, S. Golowin, K. Banik, G.K. Fenton, G.S. Daehn, Coupling Experiment and Simulation in Electromagnetic Forming Using Photon Doppler Velocimetry, steel research international, 80 (2009) 359-365.
[28] Y. Zhang, S. Babu, G. Daehn, Interfacial ultrafine-grained structures on aluminum alloy 6061 joint and copper alloy 110 joint fabricated by magnetic pulse welding, Journal of Materials Science, 45 (2010) 4645-4651.
[29] N. Hutchinson, Y. Zhang, G. Daehn, K. Flores, Solid state joining of Zr-based bulk metallic glass, in: TMS 2009 Annual Meeting and Exhibition, TMS, San Francisco, (2009).

[30] M. Watanabe, S. Kumai, G. Hagimoto, Q. Zhang, K. Nakayama, Interfacial microstructure of aluminum/metallic glass lap joints fabricated by magnetic pulse welding, Materials transactions, 50 (2009) 1279-1285.
[31] M. Kashani, T. Aizawa, K. Okagawa, Y. SUGIYAMA, Welding of Manganin and Copper sheets by Using Magnetic Pulse Welding (MPW) Technique, IEICE technical report EMD, 109 (2009) 29-31.
[32] T. Aizawa, K. Okagawa, M. Kashani, Application of magnetic pulse welding technique for flexible printed circuit boards (FPCB) lap joints, Journal of Materials Processing Technology, 213 (2013) 1095-1102.
[33] A. Stern, O. Becher, M. Nahmany, D. Ashkenazi, V. Shribman, Jet Composition in Magnetic Pulse Welding: Al-Al and Al-Mg Couples MPW jet phenomena were investigated and jet material cornposition for similar Al alloys and two samples of dissimilar Al-Mg alloy couples were observed, Welding journal, 94 (2015) 257S-264S.
[34] V. Shribman, Magnetic Pulse welding for dissimilar and similar materials, in: 3rd International Conference on High Speed Forming, Dortmund, (2008) 13-22.
[35] V. Shribman, Y. Livshitz, O. Gafri, Magnetic pulse welding and joining–a new tool for the automotive, SAE Technical Paper, (2001) 3401-3408.
[36] A.K. Jassim, Magnetic pulse welding technology, in: Energy, Power and Control (EPC-IQ), 1st International Conference, Basra, (2010) 363-373.
[37] R.N. Raoelison, T. Sapanathan, N. Buiron, M. Rachik, Magnetic pulse welding of Al/Al and Al/Cu metal pairs: Consequences of the dissimilar combination on the interfacial behavior during the welding process, Journal of Manufacturing Processes, 20, Part 1 (2015) 112-127.
[38] R. Raoelison, N. Buiron, M. Rachik, D. Haye, G. Franz, M. Habak, Study of the elaboration of a practical weldability window in magnetic pulse welding, Journal of Materials Processing Technology, 213 (2013) 1348-1354.
[39] Z. Fan, H. Yu, C. Li, Plastic deformation behavior of bi-metal tubes during magnetic pulse cladding: FE analysis and experiments, Journal of Materials Processing Technology, 229 (2016) 230-243.
[40] Standard Practice for Conducting Force Controlled Constant Amplitude Axial Fatigue Tests of Metallic Materials, in: ASTM E466-07, ASTM International, West Conshohocken, PA, (2007).
[41] I. Çaldichoury, P. L'Eplattenier, EM Theory Manual, in: Electromagnetism and Linear Algebra in LS-DYNA, Livemore Software Technology Corporation, 2012.
[42] W.H. Hayt, J.A. Buck, Engineering electromagnetics, McGraw-Hill New York, (2001).
[43] T. Sapanathan, K. Yang, D. Chernikov, R.N. Raoelison, V. Gluschenkov, N. Buiron, M. Rachik, Thermal Effect during Electromagnetic Pulse Welding Process, in: Materials Science Forum, Trans Tech Publ, (2017) 1662-1667.
[44] S. Al-Hassani, J. Duncan, W. Johnson, On the parameters of the magnetic forming process, Journal of Mechanical Engineering Science, 16 (1974) 1-9.

[45] B. Kinsey, A. Nassiri, Analytical model and experimental investigation of electromagnetic tube compression with axi-symmetric coil and field shaper, CIRP Annals, 66 (2017) 273-276.
[46] A. Mamalis, D. Manolakos, A. Kladas, A. Koumoutsos, Electromagnetic forming tools and processing conditions: numerical simulation, Materials and Manufacturing Processes, 21 (2006) 411-423.